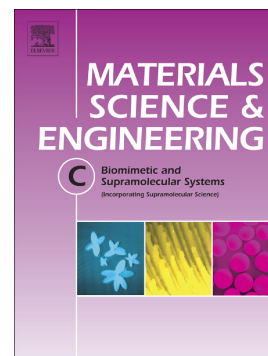


## Journal Pre-proof

Fabrication of 3D hybrid scaffold by combination technique of electrospinning-like and freeze-drying to create mechanotransduction signals and mimic extracellular matrix function of skin

Azadeh Izadyari Aghmiuni, Saeed Heidari Keshel, Farshid Sefat, Azim Akbarzadeh Khiyavi



PII: S0928-4931(20)33671-7

DOI: <https://doi.org/10.1016/j.msec.2020.111752>

Reference: MSC 111752

To appear in: *Materials Science & Engineering C*

Received date: 24 April 2020

Revised date: 16 October 2020

Accepted date: 21 November 2020

Please cite this article as: A.I. Aghmiuni, S.H. Keshel, F. Sefat, et al., Fabrication of 3D hybrid scaffold by combination technique of electrospinning-like and freeze-drying to create mechanotransduction signals and mimic extracellular matrix function of skin, *Materials Science & Engineering C* (2020), <https://doi.org/10.1016/j.msec.2020.111752>

This is a PDF file of an article that has undergone enhancements after acceptance, such as the addition of a cover page and metadata, and formatting for readability, but it is not yet the definitive version of record. This version will undergo additional copyediting, typesetting and review before it is published in its final form, but we are providing this version to give early visibility of the article. Please note that, during the production process, errors may be discovered which could affect the content, and all legal disclaimers that apply to the journal pertain.

# Fabrication of 3D hybrid scaffold by combination technique of electrospinning-like and freeze-drying to create mechanotransduction signals and mimic extracellular matrix function of skin

Azadeh Izadyari Aghmiuni<sup>a,\*</sup>, Saeed Heidari Keshel<sup>b,c,\*</sup>, Farshid Sefat<sup>d,e</sup>, Azim Akbarzadeh Khiyavi<sup>a</sup>

<sup>a</sup> Department of Nanobiotechnology, Pasteur Institute of Iran, Tehran, Iran.

<sup>b</sup> Medical Nanotechnology Research Center, Shahid Beheshti University of Medical Sciences, Tehran, Iran.

<sup>c</sup> Department of Tissue Engineering and Applied Cell Science, School of Advanced Technologies in Medicine, Shahid Beheshti University of Medical Sciences, Tehran, Iran.

<sup>d</sup> Department of Biomedical and Electronics Engineering, School of Engineering, University of Bradford, Bradford, UK.

<sup>e</sup> Interdisciplinary Research Centre in Polymer Science & Technology (IRC Polymer), University of Bradford, Bradford, UK.

\*Corresponding Author: azadeh.izadyari@gmail.com (A. Izadyari Aghmiuni), saeedhey@gmail.com (S. Heidari Keshel)

## Abstract

Fabrication of extracellular matrix (ECM)-like scaffolds (in terms of structural-functional) is the main challenge in skin tissue engineering. Herein, inspired by macromolecular components of ECM, a novel hybrid scaffold suggested which includes silk/hyaluronan (SF/HA) bio-complex modified by PCP: [polyethylene glycol/chitosan/poly( $\epsilon$ -caprolactone)] copolymer containing collagen to differentiate human-adipose-derived stem cells into keratinocytes. In followed by, different weight ratios (wt%) of SF/HA (S1:100/0, S2:80/20, S3:50/50) were applied to study the role of SF/HA in the improvement of physicochemical and biological functions of scaffolds. Notably, the combination of electrospinning-like and freeze-drying methods was also utilized as a new method to create a coherent 3D-network. The results indicated this novel technique was led to ~8% improvement of the scaffold's ductility and ~17% decrease in mean pore diameter, compared to the freeze-drying method. Moreover, the increase of HA (~20wt%) increased porosity to 99%, however, higher tensile strength, modulus, and water absorption% were related to S2 (38.1, 0.32 MPa, 75.3%). More expression of keratinocytes along with growth pattern similar to skin was also observed on S2. This study showed control of HA content creates a microporous-environment with proper modulus and swelling%, although, the role of collagen/PCP as base biocomposite and fabrication technique was undeniable on the inductive signaling of cells. Such a scaffold can mimic skin properties and act as the growth factor through inducing keratinocytes differentiation.

**Keywords:** ECM components, Skin tissue engineering, Composite scaffolds, Fabrication techniques, Keratinocytes.

## 1. Introduction

The skin is one of the most important organs of the human body that controls body functions such as the elimination of toxins, prevention of water loss, protection from other organs against external agents, and mechanical stress. This high proliferating tissue is usually able to regenerate small wounds. Nonetheless, the extent of the wound and creation of large full-thickness lesions, burn injuries, chronic wounds, diabetic foot ulcers, bedsore (pressure ulcers), etc. considerably hamper the self-healing process of the skin and create serious and negative effects on the quality of life [1–3]. Therefore, regardless of the nature of the causative agent, appropriate coverage is needed for the acceleration of the wound healing process to prevent infection and promote the quality of skin regeneration (a scar-free). In the last decades, routine surgical skin grafting techniques such as autograft, allograft, and xenograft were applied for remodeling skin, but there were several limitations especially regarding donor sites and high risk of immune rejection [4,5].

The recent years, regenerative medicine as novel science provides engineered skin substitutes to circumvent these problems [6,7], by promoting cell differentiation into skin cells, increasing interactions of cell-to-cell and cell-to-substrate, secretion of growth factors to drive re-epithelialization and skin remodeling [8,9]. In this field, tissue engineering techniques along with stem cells (SCs) and polymers act as a new approach accelerates the wound healing process when the skin is not able to repair itself [10–12].

Among the types of SCs, adipose-derived stem cells (ASCs) have been recognized as the main cellular source for tissue engineering and regenerative medicine applications, due to their properties of multipotent (i.e. able to differentiate into keratinocytes, fibroblasts, osteoblasts, neural cells, etc.), extensive proliferation ability [13–17], ease of isolation from subcutaneous adipose tissue, hypoinflammatory and least ethical problem [15–18]. However, the application of ASCs in regenerative medicine will be successful when suitable conditions are provided for their interactions control and differentiation into the target tissue such as skin. To this aim, the types of natural and synthetic polymer and their combination (in the scaffold form and as supporting structures and replace of wound temporary-ECM<sup>1</sup>) are used [19–24]. The ultimate goal of these engineered scaffolds is to create an ideal substrate for remodeling natural ECM and provide optimal conditions for improving the differentiation of stem cells into desired cells [25,26]. Therefore, such the engineered scaffold that mimics ECM activity can be highly interesting, especially when designed for replacing skin tissue and its regeneration. In this field, the ideal scaffolds should possess suitable characteristics such as biocompatibility, micropore size, porosity above 95%, controllable biodegradability, and suitable mechanical properties to improve cell interactions and differentiation into the skin cells [27]. Therefore, biomaterials are one of the logical choices for scaffold design and the skin ECM simulation. In this field, collagen is the most known ECM proteins which used widely in tissue-engineered constructs due to the low processability (at room temperature and high hydrophilic nature), biocompatibility, and excellent biological properties like cell adhesion and proliferation expansion [28,29]. Although, some of its physicochemical properties like the fast biodegrading rate, the low mechanical and thermal resistance limit the

---

<sup>1</sup> Extracellular matrix

use of collagen in tissue engineering [30], however, modification of this natural polymer by cross-linking or combining with other polymers is an effective method to optimize its properties [30,31]. Chitosan that is very similar in terms of chemical structure to the glycosaminoglycans (GAGs) can play an important role in this field [32]. This biomaterial due to hydroxyl (-OH) and amine (-NH) functional groups can link to other polymers to make a copolymer, or act as a bridge to increase the efficiency of cross-linkers and modify the limit of the use of other biopolymers such as collagen for application of tissue engineering [30,33]. Moreover, repetitive proteins in silk fibers (SF) structure due to the short side-chain amino acids such as glycine and alanine can act like proteoglycans of ECM [34], as well as, due to the dominance of hydrophobic domains between the chains create a  $\beta$ -sheet structure which improves the elastic properties and strength of silk fibers similar to elastin role in the natural ECM [35–37]. These properties play an important role in the engineered scaffolds of the skin and enhance module and stress-strain of scaffold [38]. However, the large hydrophobic domains in silk fibroin that dominate its structure decrease bonding and increase degradation rate [39]. It seems that hyaluronan or hyaluronic acid (HA) as the most important linear polysaccharide or glycosaminoglycans of the ECM can partially solve this problem [40–42]. This biomaterial maintains the structural integrity of ECM in the scaffolds when interacting with proteins and proteoglycans such as collagen and silk. HA as a signaling molecule plays a key role in cell interactions and tissue remodeling through communication with a variety of cell surface receptors and the binding proteins [43,44]. However, there are limitations such as the poor mechanical properties and rapid enzymatic degradation for using natural polymers while high mechanical strength and suitable elasticity are required for designing skin scaffolds. The synthetic polymers such as polyethylene glycol (PEG) and poly ( $\epsilon$ -caprolactone) (PCL) can be effective in this field. Indeed, PEG provides an appropriate biological signal in the tissue-engineered scaffolds which is resulted from incorporated proteins, polysaccharides or peptides and can increase the adhesion of the seeded cells on the scaffold due to possessing these ligands of cell adhesion [45–49]. Further, PCL can lead to maintaining the physical integrity of the scaffold into the intracellular water<sup>2</sup> and improving the mechanical strength and stiffness of the scaffold [50–53]. Indeed, its ability to suitable miscibility with other polymers such as chitosan helps to maintain the physical strength of the scaffold [52] and decreases the problem of the in-depth penetration of cells in the scaffold [54].

In addition to choosing the type of polymers, the techniques of the scaffold design are also known as one of the main factors that can be effective in remodeling the ECM network. In this field, uncontrolled freeze-drying leads to the creation of a non-uniform freezing process and consequently a heterogeneous structure [55], likewise, the main disadvantage of the electrospinning method is the involvement of toxic organic solvents during scaffold preparation, which can be harmful to cell bioactivity. It seems that the combination of these two techniques not only will be able to remove the mentioned problems but also may provide a 3D-scaffold which possesses the advantages of all two methods.

---

<sup>2</sup> Intracellular water is the water located inside cells that containing all the necessary biological molecules including the proteins and nucleic acids.

Accordingly as described above, in this research, a combination of natural and synthetic polymers are used to create a native ECM-like scaffold with optimal combination properties such as strength, durability and compatibility, controlled degradability, and good modulus along with in-depth penetration of cells to provide enhance cells adhesion and create mechanotransduction signals for improving cell-cell and cell-scaffold interactions, and regulate cellular activities such as stem cell proliferation and their differentiation into the skin cells (like keratinocytes) and wounds healing. The polymers used in the structure of the hybrid porous scaffolds include SF/HA bio-complex modified by PEG/chitosan/PCL biocomposite containing collagen. Various weight ratios of SF and HA were used for studying their effectiveness in the structural network and physicochemical and mechanical properties of scaffold and stem cell differentiation rate into keratinocytes. Human-ASCs were also selected to investigate their differentiation potential into keratinocytes, because of ease of isolation and hypoimmunogenic. It is notable that the combination technique including the methods of electrospinning-like (polymers complex was injected with the linear reciprocating motion, in the opposite directions and the harmonic circumferential motion into the 48-well plates by 1ml syringe, 29- gauge, Red) and freeze-drying (with a two-stages freezing process to control freezing temperature and subsequently pores size) was used to fabricate the engineered scaffold. Finally, the physicochemical, mechanical, and biological assay was carried out to evaluate the characterization of the scaffolds and analyze the results of cell differentiation on the scaffolds prepared with the combination technique of the electrospinning-like and freeze-drying, as well as freeze-drying method.

## 2. Materials and methods

### 2.1. Materials

Chitosan (CS) with an average molecular weight (Mn) of 234 kDa and an average deacetylation degree of 95%, PCL (average Mn: 45000), PEG (average Mn: 6000), acetic acid, hyaluronan (hyaluronic acid: HA), 1-Ethyl-3-[3-dimethylaminopropyl]carbodiimide hydrochloride (EDC), N-hydroxysuccinimide (NHS), bovine collagen solution (Acid-soluble collagen; ASC, Type I), MTT (tetrazolium salt 3-(4, 5-dimethylthiazol- 2-yl)-2,5-diphenyltetrazolium bromide) and dimethyl sulfoxide (DMSO) were commercially obtained from Sigma-Aldrich (Sigma Co., St. Louis, USA). Dulbecco's modified eagle medium (DMEM), bovine serum albumin (BSA), and fetal bovine serum (FBS) were also obtained from Gibco (Massachusetts, USA). All other chemicals were from Sigma-Aldrich (St. Louis, MO) and Bombyxmori was obtained from the domestic producer, AbrishamGuilan Co., Iran.

### 2.2. Preparation of SF solution

To prepare 3 wt% (w/v) silk fibroin solution, in accordance with the procedures previously pieces of raw Bombyxmori silk fibers were immersed in 0.02 molar solution of sodium carbonate ( $\text{Na}_2\text{CO}_3$ ) with 0.05 wt% (w/w) (at  $100 \pm 2^\circ\text{C}$ , 30 min) to remove sericin. This process was repeated three times for degumming the fibers completely. Then, the extracted silk fibroin fibers were rinsed with  $\text{diH}_2\text{O}$  (deionized water) to remove  $\text{Na}_2\text{CO}_3$

residues and dried at 25°C overnight. Thereafter, the fibers dissolved with 10% (w/v) in the solution of CaCl<sub>2</sub>: CH<sub>3</sub>CH<sub>2</sub>OH: H<sub>2</sub>O with a mole ratio of 1:2:8 (70 ± 2°C) and mixed on a magnetic stirrer for 3 h. Then, the solution was dialyzed against diH<sub>2</sub>O using a dialysis membrane (cellulose membrane, Viscofan 22 EU – 20 USA) at 8°C for 96 h to remove the salts of the solvent and filtered to remove impurities and aggregates. The final concentration of SF aqueous solution was obtained 3.2 wt% by weighing the remaining solid after drying. Notably, the dialysis water was changed every 24 h. Finally, this solution was diluted to 3 wt% with diH<sub>2</sub>O and stored at -80°C.

### 2.3. Preparation of SF/HA solution

The 1.0 wt % hyaluronan (HA) aqueous solution was obtained by dissolving HA powder in cold diH<sub>2</sub>O for 24 h. Then, the various weight ratios of SF/HA were prepared by mixing 3 wt % SF solution and 1.0 wt % HA solution at 4-8°C for 24 h. The volume ratios of SF/HA (SH) in mixed solutions were 100/0, 80/20, 50/50 (v/v), respectively. Finally, the mentioned solutions were sonicated by a bath sonicator (Bandelin Sonorex Digitec, 35 kHz) for 10 min at 30°C to improve electrostatic, hydrogen, or van der Waals interactions between the SF and HA.

### 2.4. Preparation of PEG/Ch/PCL solution

A ternary solution of PEG/Chitosan/PCL (PCP) with a mass ratio of 5:3:1 was prepared by mixing PEG solution (6 wt% in diH<sub>2</sub>O, 25°C, 24 h), chitosan solution (5 wt% in 0.5 M acetic acid, 25°C, 24 h) and PCL solution (3 wt% in 60% acetic acid, 40°C, 24 h). Over the preparation of the ternary solution, NHS and EDC were separately dissolved in PEG solution and PCL solution with 10 and 20 wt% respectively. NHS, the activator of -OH group and EDC, creates an ideal condition for cross-link reaction. Finally, the PCL solution was added to the mixed solution of PEG/Chitosan and stirred for 24 h at room temperature.

### 2.5. Preparation of SH/Collagen/PCP scaffold

To prepare SH/Collagen/PCP hybrid scaffolds, solutions of SH and PCP with a volume ratio 1:1 were simultaneously injected into the 48-well plates, which were placed on a shaker-linear bearing (with the linear reciprocating motion), by means of a syringe pump (SP1000HSM, Fanavaran Nano Meghyas, Iran) and 1ml syringe (29 gauge, Red, 12.7-mm needle length, 0.33-mm nominal diameter) with the injection rate of 15 µl/min. Then, collagen (0.5 mg/ml, pH=7.2) was injected on the SH/PCP solutions (into the 48-well plates) to create 3% weight ratio against the total weight of SH/PCP (Fig. 1). Finally, the electrospun-like solutions (entire polymeric solution) were respectively frozen at -20°C for 24 h and -80°C for 48 h (to control pores size) [5]. Then they were lyophilized (freeze-dried) for 72 h to prepare porous 3D-scaffolds.

The collagen/PCP scaffold was also prepared in the same manner to study the effect of SF and HA in the scaffold structures and functions. Moreover, to evaluate the role of the electrospinning-like method combined with freeze-drying, the physicochemical properties



of the collagen/PCP scaffold were compared with our previous study (the fabricated collagen/PCP scaffold with the freeze-drying method) [5]. Finally, the scaffolds were stored at 4-8°C to study the biological behavior of cells on the scaffold. The surface and thickness of scaffolds were respectively determined about 10 mm and 5 mm.

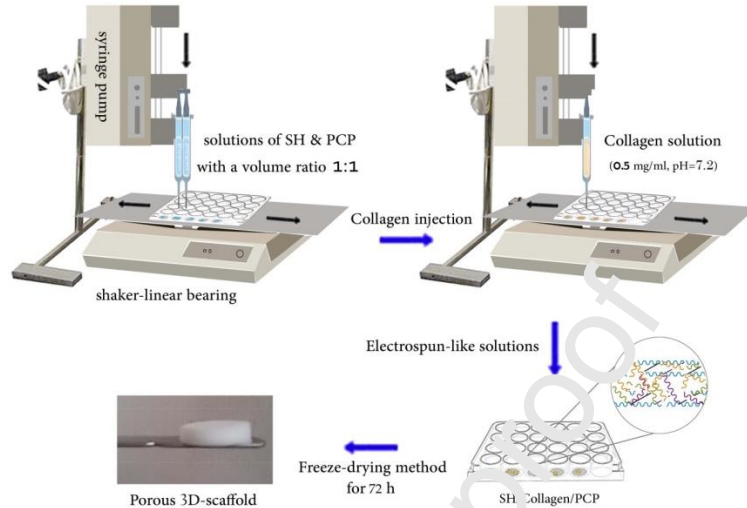


**Figure 1.** Schematic of the porous 3D-scaffold preparation process.

## 2.6. Fourier-transform infrared spectroscopy (FTIR) study

Chemical characterization and FTIR spectroscopic analysis of porous scaffolds were performed with FTIR (Model-ALPHA, Bruker, Germany) spectrometer over the wavenumber range of 400–4000  $\text{cm}^{-1}$  at a resolution of 4  $\text{cm}^{-1}$  with 16 scans per scaffold. The spectra of scaffolds were measured after mixing potassium bromide (KBr) with powdered scaffolds at 1:1 ratio and pressing into a pellet.

## 2.7. Water absorption

The water absorption properties of the scaffolds were measured according to a previous method [56–58]. Briefly, the dry scaffolds (10 mm diameter and 5 mm thickness) were first weighed ( $W_d$ ) and then immersed in a phosphate-buffered saline solution (PBS, pH 7.4) and incubated *in vitro* at 37°C for 24 h. Afterward, excess water was removed and the weight of the scaffolds was recorded as wet weight at pre-determined time intervals ( $W_w$ ). To study water retention, the water-saturated scaffolds were first placed into the filter paper for 3 min to remove excess water and weighed immediately ( $W'_w$ ). The swelling ratio, the percentage of water uptake, and the water retention ability were respectively obtained by Equations 4, 5, and 6 [59,60]. Data from each scaffold were obtained using three measurements ( $n=3$ ) and were expressed as mean  $\pm$  SD.

$$\text{Swelling} = \frac{W_w - W_d}{W_d} \quad \text{Eq. (1)}$$

$$\text{Water uptake} = \frac{W_w - W_d}{W_w} \times 100 \quad \text{Eq. (2)}$$

$$\text{water retention} = \frac{W'_w - W_d}{W_d} \times 100 \quad \text{Eq. (3)}$$

## 2.8. Enzymatic *in vitro* degradation

The rate of scaffolds biodegradation was analyzed by a lysozyme degradation test [57,61]. In brief, the initial dry weight of the scaffolds ( $W_i$ ) was recorded. Then, scaffolds were immersed into a 4-well plate having PBS (pH 7.4) containing lysozyme (500 $\mu$ g/ml) and incubated at 37°C. At predetermined time intervals (every 4 days), the scaffolds were removed from the degradation medium, washed twice with distilled water, frozen at -80°C, lyophilized for 1 day, and weighed ( $W_t$ ). The biodegradation of scaffolds was observed to evaluate the scaffold weight loss (degradability) for 14 days under simulated physiological conditions (mean  $\pm$  SD, n=3). Equations 7 and 8 were used to calculate the percentage of degradation (D%) and weight remaining, respectively (WR%) [61,62].

$$D\% = \frac{W_i - W_t}{W_i} \times 100 \quad \text{Eq. (4)}$$

$$WR\% = 100 - \left[ \frac{W_i - W_t}{W_i} \times 100 \right] = \frac{W_t}{W_i} \times 100 \quad \text{Eq. (5)}$$

## 2.9. Mechanical behavior

The mechanical properties of the lyophilized scaffolds (10 $\times$ 5 $\times$ 2 mm<sup>3</sup>) were determined by a tensile tester instrument (Zwick/Roell, 1446, Germany) at 25°C. Briefly, the mentioned scaffolds were placed between the two grips of gage and thoroughly hydrated by spraying with PBS (pH 7.4). Then, the stretching speed of the instrument was set at 2 mm/min. The elastic limit, Young modulus, MPa, ultimate tensile strength (UTS), and breaking strain% were calculated from the resultant engineering stress/strain curves, according to the regulations in ASTM D3039 [63]. Notably, five specimens were evaluated for each scaffold and the values were expressed as mean $\pm$  SD (n=5).

## 2.10. Microstructural observation and scaffold porosity

The morphology and microstructure study of the lyophilized scaffolds and cells were observed using a scanning electron microscope (SEM) (XL30 ESEM, Philips, Germany). The surface of the scaffolds was coated with a thin film of gold and imaged at an accelerating voltage of 20.0 kV. The pore size of scaffolds was measured from SEM images by Clemex Vision with at least 80 pores per scaffold.

In followed by, the liquid displacement method was used to determine the porosity of scaffolds and absolute ethanol was selected as a displacement liquid for its easy penetration



into the pores of the scaffold without shrinking or swelling its structure [64]. In this test, the scaffolds, empty pycnometer, and ethanol were kept at 25°C for 1 h. Then, the pycnometer was filled with absolute ethanol and its weight was recorded as  $W_1$ .

Moreover, lyophilized scaffolds with a known weight ( $W_S$ ) were separately immersed into the pycnometer then the bottle was submerged slowly to remove all the air in the porous scaffold. Thereafter, the pycnometer was refilled with ethanol and weighed after 5 min ( $W_2$ ). Subsequently, the saturated scaffold with ethanol was removed from the bottle and the pycnometer weight was recorded as  $W_3$ . At the end, the volume of the scaffolds ( $V_S$ ) and the total volume of the pores ( $V_P$ ) were obtained by using Equations 1 and 2, respectively. Then, the porosity of scaffolds determined with Equation 3. Values were represented as the mean  $\pm$  standard deviation (SD) for  $n=3$ .

$$V_S = \frac{W_1 - W_2 + W_S}{\rho} \quad \text{Eq. (6)}$$

$$V_P = \frac{W_2 - W_3 - W_S}{\rho} \quad \text{Eq. (7)}$$

$$\xi = \frac{V_P}{V_P + V_S} = \frac{W_2 - W_3 - W_S}{W_1 - W_3} \quad \text{Eq. (8)}$$

The  $\rho$  and  $\xi$  are the density of absolute ethanol and the porosity of the scaffold, respectively.

## 2.11. Cells-scaffold interactions and biocompatibility

### 2.11.1. Adhesion and proliferation assay

To understand biological behavior and *in vitro* biocompatibility assessment of scaffolds, the polymeric samples (10 mm diameter  $\times$  1 mm thickness) were first placed in 96-well plate (Sigma-Aldrich Inc., St. Louis, MO, USA) and pressed with stainless steel rings. The scaffolds were sterilized under UV-light for 2 h and dipped in 70% alcohol solution overnight. The sterilized scaffolds were respectively washed 3 times with PBS and the cell culture medium (every 30 minutes) at room temperature. Then, the 3rd passage of human adipose-derived stem cells (h-ASCs) used in our previous study [5] was seeded onto the scaffolds ( $1 \times 10^6$  cells/well) and were covered by Dulbecco Modified Eagle Medium–Low Glucose (DMEM-LG) containing 10% FBS, and penicillin 100 U/ml-streptomycin 1000 U/ml (Gibco, Massachusetts, USA). Afterward, the plates were incubated at 37°C, 5% carbon dioxide ( $\text{CO}_2$ ), and 95% humidity for 5, and were observed under SEM to assess initial adhesion (cell/scaffold interactions), after 5 h of the culture on the scaffolds. Briefly, the h-ASCs-loaded scaffolds were washed with PBS (2 times) and cells were fixed using 2.5% glutaraldehyde solution. After 30 min, the samples were washed again with PBS, and post-fixation was carried out with 1% Osmium tetroxide. The samples were dehydrated in ascending concentrations (i.e., 30, 50, 70, 90, and 100%) of ethanol solutions, for 5 minutes at each concentration. Finally, the samples were dried in the open-air and were mounted on copper stubs, coated with gold, and observed by SEM (accelerating voltage of 10.0 kV).

To evaluate the distribution and proliferation of h-ASCs on the scaffolds, the cells were also observed by SEM after an additional 48 h of incubation under the same conditions. The culture medium was changed every day.

#### 2.11.2. Cell viability assay

The viability of h-ASCs onto the scaffolds and control group (medium without scaffolds) was assessed by cell proliferation and viability assay. In brief, h-ASCs at a plating density of  $1 \times 10^4$  cells/well were seeded onto scaffolds in 96-well plate. After 24, 48 h of culture, 20  $\mu$ l of the MTT (Sigma, US) at the final concentration of 2.5 mg/ml was added to each well and incubated in a humidified atmosphere with 5% CO<sub>2</sub> at 37°C, for an additional 4 h. Then, the medium was removed, and the cells were solubilized in 100  $\mu$ l of dimethyl sulfoxide (DMSO, Sigma, US) and absorbance was measured at a wavelength of 570 nm. The cell viability in the control group was considered 100%.

#### 2.12. *In Vitro* differentiation of h-ASCs into keratinocytes

The culture-expanded h-ASCs on the scaffolds were tested for their ability to differentiate into epidermal keratinocytes. To this end, the h-ASCs were seeded in 6-well culture plates with/without scaffold, at a density of  $1 \times 10^6$  cells/well. Notably, DMEM-LG supplemented with 10% FBS, containing 1% Pen-Strep (penicillin-streptomycin) (all second: Gibco, Massachusetts, USA) and 5  $\mu$ g/ml insulin, 0.5  $\mu$ g/ml hydrocortisone, 1.5 mM calcium chloride, and 10 ng/mL keratinocyte growth factor (KGF) (Sigma- Aldrich Inc., St. Louis, MO, USA) was used as specific induction medium to differentiate cell onto plates without scaffold (as the control group). The culture medium without insulin, hydrocortisone, calcium chloride, and KGF was also added to the cells which seeded onto the scaffolds. Finally, cells were cultivated in standard conditions for 14 days and the medium was changed every other day. After 7 and 14 days in culture, the expression of two epithelial markers (keratinocytes 10 and 14: KRT10 and KRT14) and cell morphologies (round or polygonal shape) were assessed by real-time PCR<sup>3</sup> and ICC.

#### 2.13. Real-time PCR analysis

To analyze specific gene expression in all scaffolds, total RNA was isolated from cultured cells on the scaffolds by an RNA extraction kit (Takara, Tokyo, Japan). For this aim, the RNA samples were treated with DNase I (Takara, Tokyo, Japan) to avoid the genomic DNA (gDNA) contamination. The isolated RNA quantity was evaluated by nanospectrophotometry (NanoDrop; Thermo, Wilmington, USA). For reverse transcription, 2  $\mu$ g of total RNA was used with the Revert Aid-first strand cDNA synthesis kit (Takara, Tokyo, Japan). The RNA extracted from the human normal skin cell line (NCBI Code: C192, Iranian Pasture Institute cell bank, Tehran, Iran) was applied as a positive control. The real time-PCR (Rotor-Gene Q Real-Time PCR System, Qiagen, USA) reaction was carried out with SYBR

---

<sup>3</sup> Polymerase Chain Reaction

Premix Ex Taq™ (Takara BIO, INK, Japan) which uses Taq Fast DNA Polymerase, SYBR Green I dye to detect double-stranded DNA. The reaction was performed using the following program; 5 minutes of 95°C (enzyme activation), 20 seconds at 95°C (initial denaturation), 40 seconds (annealing temperature), and 1 minute of 72°C (extension), followed by 40 cycles with a final extension at 72°C. The final stage comprises the analysis of the melt curve through a denaturing step (15" at 95°C), followed by annealing (1' at 60°C) and ramping to 95°C with 0.3°C increment/step. The expression level of the genes was normalized to human  $\beta$ -actin as a housekeeping gene and quantified using the  $2^{-\Delta\Delta Ct}$  method. Statistical analysis was performed using ANOVA and p-value < 0.05 was considered to be significant. The level of candidate genes in different sample types was compared by the Fisher LSD test. The primer sequences (5'→3') were used as below: KRT10 (Accession no: NM\_000421.3), forward: ACTACTCTTCCTCCCGCAGT and reverse: CAGAGCTCCCACGGCTAAAA (Tm= 60 °C); KRT14 (Accession no: NM\_000526.4), forward: AGACCAAAGGTCGCTACTGC and reverse: ATCGTGCACA TCCATGACCT (Tm= 60 °C), and  $\beta$ -actin (ACTB) (Accession no: NM\_001101.4), forward: GGCGCCCTATAAAACCCAGC and reverse: GCTCGATGGGGTACTTCAGG (Tm= 60 °C).

#### 2.14. Immunocytochemistry (ICC) assay

For this assay, cultured h-ASCs on the sterilized scaffolds (at days 7 and 14) were washed with PBS (3 times). Then, endogenous peroxidase activity was inactivated by 3% H<sub>2</sub>O<sub>2</sub> (hydrogen peroxide), and plates were incubated in a blocking solution, consisting of 1% BSA for 1 h, to block non-specific sites. Afterward, the cells were washed again with PBS and incubated with primary antibodies (Anti-Cytokeratin 10 antibody [RKSE60] (ab9025) and Anti-Cytokeratin 14 antibody [IL002] (ab7800) at 4°C, overnight. After being labeled with the primary antibody, the cells were incubated with FITC-conjugated anti-rabbit IgG (BD Pharmingen™), for 2 hr. Finally, immunoreactive cells were visualized by fluorescent microscopy (LabPro CETL, Oxford).

#### 2.15. Statistical analysis

All experiments were conducted at least three times (n = 3) and all values were described as the mean  $\pm$  SD. Statistical analysis was performed by the T-Test and one-way analysis of variance (one-way ANOVA), Dunnett t-tests, and Scheffe's post hoc test in IBM SPSS Statistics 24 software and p < 0.01, p < 0.05, and p < 0.001 were considered as statistically significant.

### 3. Results and discussion

#### 3.1. FTIR spectrum analysis

The FTIR spectra of collagen/PCP, S1, S2, and S3 were presented in Fig. 2. As the spectra show, peaks at 3423.17 cm<sup>-1</sup>, 3421.49 cm<sup>-1</sup>, 3417.94 cm<sup>-1</sup>, and 3424.42 cm<sup>-1</sup> were

respectively recorded for S1, S2, S3, and collagen/PCP, due to the existing of the -OH stretching vibrations for strong hydrogen-bonding interactions with the neighboring carboxylic groups which may be presented in the PCP-based materials and SF. Likewise, the C-H stretching vibrations were observed at  $2887.36\text{ cm}^{-1}$ ,  $2887.48\text{ cm}^{-1}$ ,  $2885.81\text{ cm}^{-1}$ , and  $3887.33\text{ cm}^{-1}$ , respectively. The range change of the peaks is attributed to chemical interactions between the copolymer containing collagen (collagen/PCP) and SF or HA. Although, it is observed that C-H and O-H absorption bands intensity is reduced in the spectra of collagen/PCP, S1, and S3 than spectrum S2 (Fig. 2a). It could be due to existing of stronger bonding inside the networks (for S2), higher content of HA in the structure of S3, and lower interaction between collagen and PCP hybrid copolymer (in collagen/PCP and S1).

There was a noteworthy point in the evaluation of spectra that related to the N-H stretching vibrations. It has shown that incorporation of HA into the PCP-based material containing collagen and SF increases the accumulation of NH band and water absorption of the scaffold. It is well-known that in line with the strengthening of the N-H band at  $3092.74\text{ cm}^{-1}$  in the S3 spectrum, the intensity of the mentioned peak was reduced in the S2 spectrum and completely missing in the S1 and collagen/PCP spectra. This could be due to the different interactions of amide and amine bands of the based materials such as chitosan and collagen with SF or SF/HA. Likewise, the peaks at  $1550\text{-}1650\text{ cm}^{-1}$  recorded for spectra, were related to amide I and II groups of collagen and chitosan which became stronger with increasing HA [65].

New absorption bands at  $2161.69\text{ cm}^{-1}$  and  $2128.36\text{ cm}^{-1}$  which were possibly corresponding to the  $\text{C}\equiv\text{C}$  or  $\text{N}=\text{C}$  bonds and exist in both S2 and S3 spectra due to the bonding of -COOH of HA with  $\text{NH}_2$  of chitosan, was completely missing in the S1 and collagen/PCP. Likewise, there were the two peaks at  $1969.72$  and  $1968.96\text{ cm}^{-1}$  for spectra S1 and S2. It means that new bands were formed via a hydrogen bond and electrostatic interactions of inner and inter-molecular of SF with other polymers, after cross-linking by EDC and NHS.

Moreover,  $1150.62$  and  $1023.55\text{ cm}^{-1}$  which are assigned to C-O asymmetric and symmetric stretching vibrations were only observed in the S3 spectrum. However, bands at  $1108.95\text{ cm}^{-1}$ ,  $1110.18\text{ cm}^{-1}$ ,  $1110.46\text{ cm}^{-1}$ , and  $1114.83\text{ cm}^{-1}$  were respectively recorded for S1, S2, S3, and collagen/PCP spectra which are attributed to C-O stretching vibrations. Other peaks were also observed at  $650\text{-}800\text{ cm}^{-1}$ ,  $840\text{-}850\text{ cm}^{-1}$ , and  $1240\text{-}1243\text{ cm}^{-1}$  exhibited respectively the C-H bending, N-H stretching vibrations, and C-N of amide and amine in every three spectra which can be a reason for the interaction of the collagen and PCP (with different intensities of the peaks) (Fig. 2 b and c). Besides the strong peaks at  $1627.60$  and  $1592.00\text{ cm}^{-1}$  in the S3 spectrum compared to other spectra could be due to excessive adding HA in the scaffold structure, which led to the weaker interactions of amide I and II groups in collagen and chitosan. Moreover, the peaks at  $1722.5\text{-}1723.77\text{ cm}^{-1}$  corresponding to the  $\text{C}=\text{O}$  stretching was observed in all spectra. This could be due to the presence of based material (PCP) and intra-/inter-molecular interactions [5].

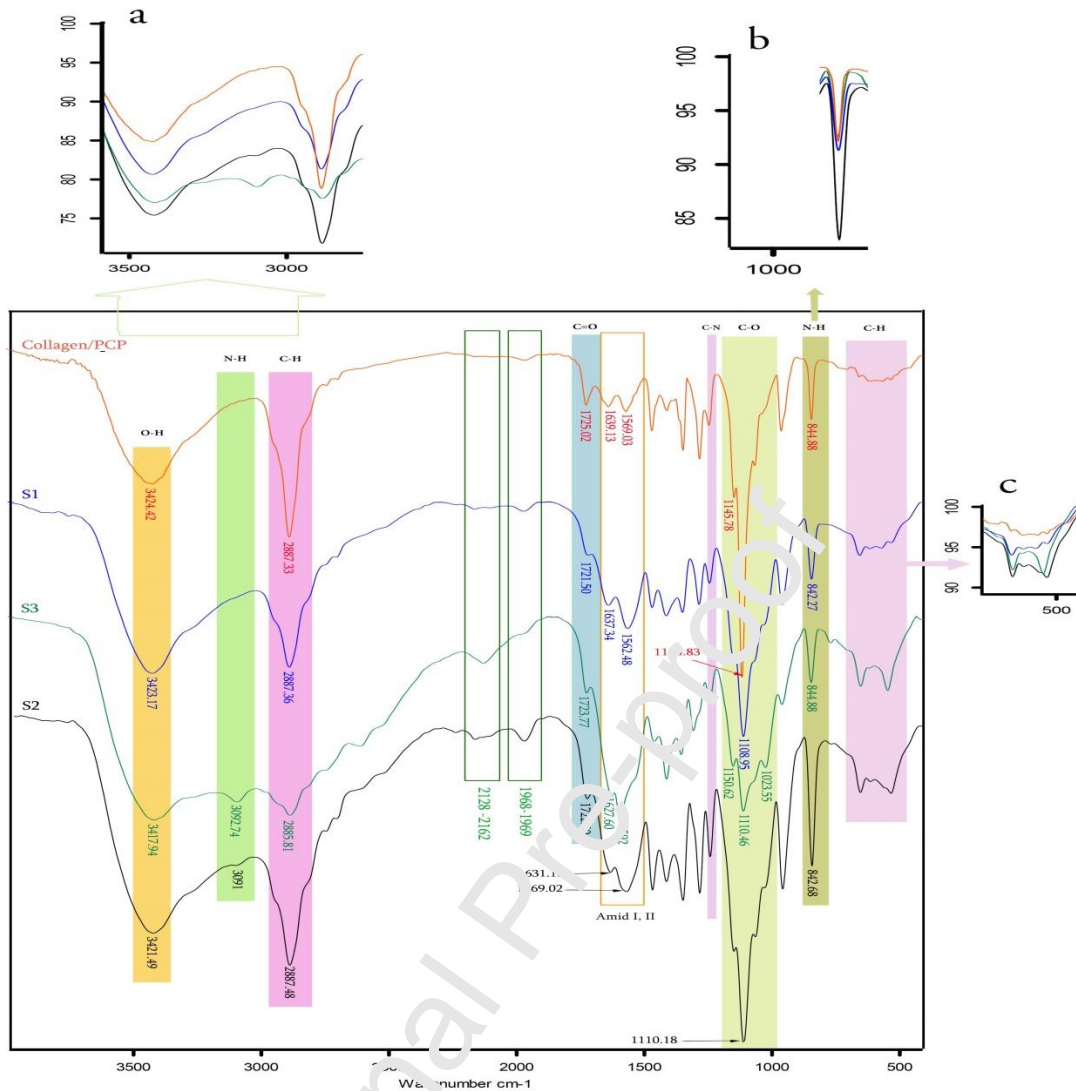


**Figure 2.** FTIR spectra for the designed scaffolds.

### 3.2. Water absorption behavior

Water absorption ability is a key factor for skin tissue-engineered scaffolds, because of the wound healing process depends on the absorption ability of the biological solution, penetration of nutrients, and transfer of metabolic waste within the biomaterials [66]. A high swelling ratio can be helpful to sustain the mentioned properties in the designed scaffolds. Hence, the swelling% of collagen/PCP scaffolds was measured and compared with our previous study [5] to evaluate the role of the electrospinning-like method combined with **the** freeze-drying technique for the preparation of scaffolds. Moreover, to study the effect of SF and HA in water absorption behavior of scaffolds, the swelling ratio and water uptake% of the hybrid porous scaffold (at various weight ratios of SF and HA) were measured after 1,2,3,5 and 24 h of incubation in PBS (Fig. 3).

As Fig. 3A shows, the combination of electrospinning-like and freeze-drying techniques was led to an increase in swelling% of the collagen/PCP scaffold in the first 10 h, as compared to the freeze-drying method ( $p < 0.05$ ). Although, there is no significant difference between the swelling% of scaffolds after 24 and 48 h, however, scaffold prepared with the

electrospinning-like and freeze-drying techniques showed the more regular swelling rate as compared to the freeze-drying technique. It can be due to the formation of new mini-bands in the mentioned scaffold network.

Our data indicated that all the scaffolds have good swelling and a high capacity to retain more water than their own weight (Table 1). So that, swelling ratio and water uptake% initially increased for all the scaffolds. This could be due to the hydrophilic chains in the scaffolds structure and a strong interaction between the PEG/chitosan/PCL hybrid biocomposite containing collagen and SF/HA complex. Although, there is a significant difference between the swelling ratio of the scaffolds, in the first hour of immersion, that related to the existence of HA and SF (Fig. 3B). So that, the swelling ratio of S3 with 50:50 weight ratios of SF: HA, after 1h was respectively 2-fold, 1.5-fold, and 3.4-fold the higher than S1 (100:0), S2 (80:80) and collagen/PCP due to the higher HA content in the scaffold structure.

However, the monitoring of water absorption over the 24-hour period showed a downtrend for the S1, S2, and S3 scaffolds as compared to collagen/PCP scaffolds that might be due to the increase in dissolution and degradation of the scaffolds (Fig. 3A, C, D, Table 1) [67].

Evaluation of this downtrend for S1, S2, and S3 scaffolds indicated that the higher weight ratio of HA (>20 wt%) led to the downtrend at a higher rate which was appeared on the line gradient of water uptake curve in Fig. 3D. So that, measuring the downtrend rate of water absorption (water uptake%) for S1, S2, and S3 during 24-hour exhibited respectively a reduction of 14.7%, 14.6%, and ~19% compared to the first hour, and S3 with the higher weight ratios of HA (50 wt%) led to the largest gradient as compared to S2 and S3, at different time intervals ( $p < 0.001$ ) (Fig. 3E). The various reports confirm that the HA content of less than 40 wt % provides stable swelling behavior [68].

Moreover, in contrast to swelling ratio after 24-hour immersion, water retention for S1 ( $214.1\% \pm 0.1$ ), S2 ( $265.6\% \pm 0.5$ ), and S3 ( $300.3\% \pm 0.5$ ) showed respectively a reduction of ~28%, 17%, and 4%. The noteworthy event in water absorption assay was less water retention of S1 and S2 versus S3 ( $P < 0.001$ ) that could be due to the large hydrophobic domains in silk fibroin that dominate the structure [39]. However, there is also the significant difference in water retention between S1 and S2 due to the presence of HA (Fig. 3F).



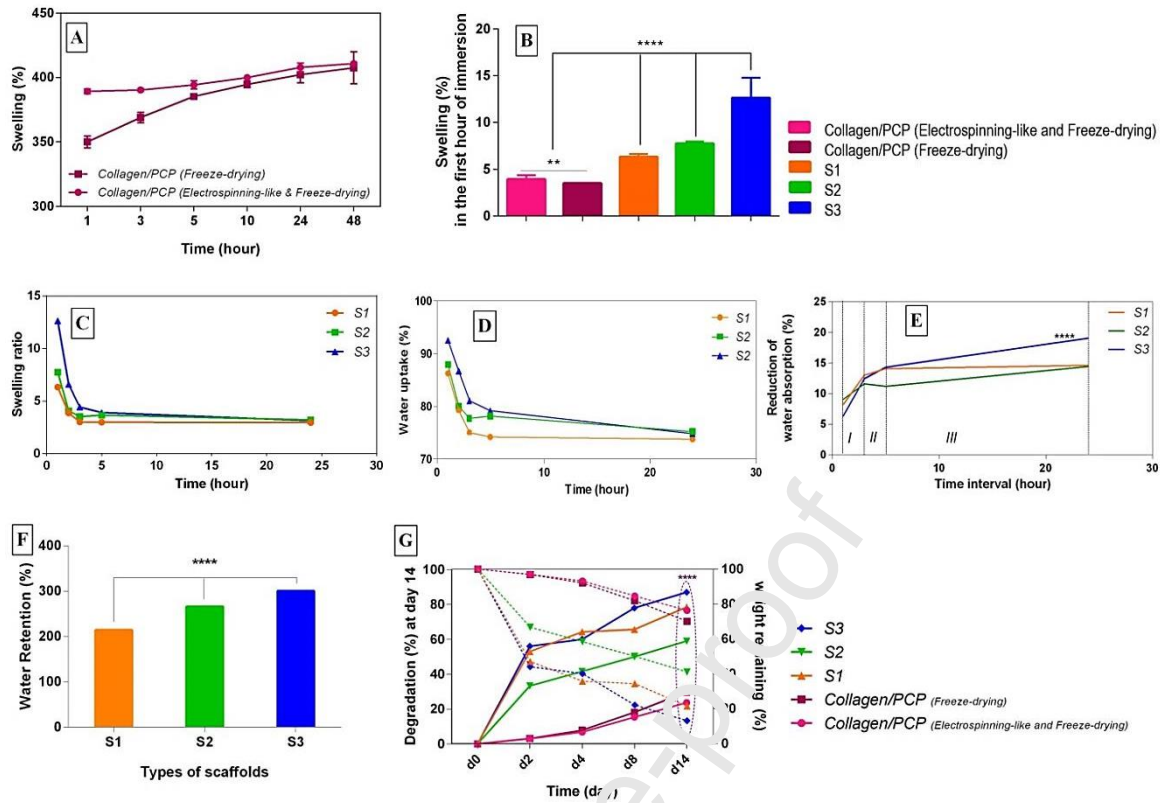


**Figure 3.** A: The swelling% for collagen/PCP (with the electrospinning-like and freeze-drying techniques) and collagen/PCP (with freeze-drying technique) [5]. B: The swelling% of the scaffold, in the first hour of immersion (\*\*\*:  $p < 0.001$ , \*\*:  $p < 0.05$ ). C and D are respectively swelling ratio and water uptake (%) ability for up to 24 hours (for S1, S2, and S3). E: line gradient of water uptake curve: there is a significant difference in the gradient of lines between S3 and two more scaffolds in each of the time interval ( $p < 0.001$ ). F: Water retention% at  $p < 0.001$ . G: Degradation behavior: dashed line and thick line show respectively degradation (%) and weight remaining (WR) ( $p < 0.001$ ).

**Table 1.** The parameters of water absorption for 3D-scaffolds.

Parameters	S1	S2	S3	Collagen/PCP (Electrospinning- like and Freeze- drying)	Collagen/PCP (Freeze-drying)
Swelling ratio (first hour)	$6.3 \pm 0.3$	$7.7 \pm 0.2$	$12.6 \pm 2.1^a$	$3.89 \pm 0.02^b$	$3.5 \pm 0.04^b$
Swelling ratio (after 24 h)	$2.9 \pm 0.9$	$3.2 \pm 1.0$	$3.1 \pm 1.0$	$4.07 \pm 0.03^c$	$4.02 \pm 0.06^c$
Water uptake% (first hour)	$86.3 \pm 0.5$	$88.2 \pm 1.0$	$92.5 \pm 1.2^a$	-	-
Water uptake% (after 24 h)	$73.6 \pm 6.4$	$75.3 \pm 6.0$	$74.8 \pm 6.0$	-	-

<sup>a</sup> The mean difference is significant at the 0.001 level.

<sup>b</sup> The mean difference is significant at the 0.05 level.

<sup>c</sup> There is no significant difference between scaffolds ( $p > 0.001$ ).

### 3.3. Degradation

The degradation behavior of the engineered scaffolds plays an important role in the process of tissue regeneration, which means that the degradation rate of scaffolds should almost match with the rate of tissue repair (14-28 days) [69]. It helps to higher mass remaining of the scaffold and consequently the available surface for cells proliferation and differentiation. Hence, the degradation profile of designed scaffolds was evaluated in PBS (pH 7.4) containing lysozyme (500  $\mu\text{g}/\text{ml}$ ) at 37°C, over 14 days. The weight remaining and degradation% curves of scaffolds are presented in Fig. 3G. As indicated in this figure, there is a significant difference in the mass loss and consequently, weight remaining between scaffolds ( $p < 0.001$ ). Such that, combination of HA and/or SF with collagen/PCP scaffolds was led to an increase in the degradation% after 14 days (collagen/PCP (freeze-drying), collagen/PCP (electrospinning-like and freeze-drying), S1, S2 and S3:  $29.88 \pm 1.1$ ,  $23.74 \pm 0.2$ ,  $78.57 \pm 1.4$ ,  $59.0 \pm 0.5$  and  $87.0 \pm 1.5$  respectively). It can be related to better interactions and the formation of stronger chemical bonds between the functional groups of collagen/PCP scaffolds in absence of SF and HA. The scaffold containing >20wt% of HA (S3) showed a higher mass-loss rate than other scaffolds (collagen/PCPs, S1 and S2,  $p < 0.001$ ), that could be due to the increase in porosity and the availability of more contact area and consequently the higher accumulation of amine (-NH) and hydroxyl (-OH) functional groups near the pore walls of the scaffold that leads to the acceleration of the hydrolytic reaction and dissolution of the scaffold during enzymatic degradation. The comparison of degradation profiles of S1 and S2 was also demonstrated that the presence of a low HA content helps to increase mass remaining% of scaffolds over a 14-day period. Indeed, the incorporation of HA (20 wt%) and SF due to the formation of hydrogen bonds can increase degradation time [68,70].

Further, our results showed, the use of the electrospinning-like technique along with the freeze-drying method can decrease the degradation% of scaffold due to better bonding of polymer chains and consequently the decrease of available sites for enzymatic and simple hydrolysis. It probably provides a proper surface for cell-scaffold interactions and the more expression of specific genes.

### 3.4. Mechanical properties analysis

The mechanical behavior of engineered scaffolds plays an important role in the improvement of cellular responses and enhancement of cell-scaffold interactions [4]. In this field, combining polymers can positively affect the biomechanical properties of the scaffold.

Here, the mechanical properties of the scaffolds were studied by the stress-strain curves (Fig. 4A). In followed by, the elastic limit, Young's modulus, maximum tensile strength (Ultimate Tensile Strength= UTS), and maximum elongation (breaking strain %) of the samples are analyzed (Table 2, Fig. 4B-D).

As Fig. 4A shows, the stress-strain curves of collagen/PCP scaffolds prepared by the combination of both methods and one method (freeze-drying technique alone), almost match so that no significant difference observed for their modulus ( $0.18 \pm 0.0$  and  $0.17 \pm 0.22$  MPa) and UTS (Fig. 4B and C, Table 2,  $p > 0.001$ ). However, maximum elongation in combining

methods illustrated ~8% increase, compared to the preparation of scaffold with one method (Fig. 4D,  $p < 0.001$ ). This could be due to a more coherent network of the scaffold, which created by the electrospinning-like technique.

When a strain of up to 1.02% is applied, the PCP fibers containing collagen for S1, S2, and S3 scaffolds remain tangled and intertwined. This amount for collagen/PCP scaffolds was recorded at about 120%, which can be related to the existence of collagen fibers that did not participate in the reactions.

Given that, the stress increases more than a strain can be said the behavior of these biocomposite scaffolds is similar to elastomers. So that, the elastic region follows a non-linear behavior (Fig. 4A), and Young's modulus is calculated via tangent of elasticity range that is the slope of the stress-strain diagram at any point. Elastic limit % and Young's modulus of scaffolds have been provided in Table 2. The results showed that combining SF with collagen/PCP was led to a significant decrease (92% and 65% respectively) in the Elastic limit % and modulus of S1 than collagen/PCP (Fig. 4B) that could be due to the lack of balance in stiffness of S1 [4]. Moreover, adding HA into the scaffolds structure increased the elastic region that can be due to the improvement of hydrophilic property and porosity of S2 (Fig. 4A and B). Although, the most stress, in the elastic region, was related to the S2. It might be because of the high resistance of the scaffold after adding HA with a lower weight ratio than SF, thereby the  $\beta$ -sheet structure of the silk protein can control water interactions and mechanobiological signaling of HA and provide mechanical integrity of scaffold [68].

Based on the reports, the skin source can affect the modulus range so that the values have been reported from  $1.8 \times 10^7 \text{ N/m}^2$  to  $10^8 \text{ N/m}^2$  [71]. These values vary among subjects, with pathological conditions, sites, and states of the muscular activities. However, Young's modulus of designed scaffolds followed the modulus of the skin (less than 0.85 MPa which has been identified as a modulus for over 30 years [72–75]). In followed by, our results showed that Young's modulus significantly decreased for both scaffolds of S1 ( $0.06 \pm 0.09 \text{ MPa}$ ) and S3 ( $0.08 \pm 0.10 \text{ MPa}$ ) than S2 ( $0.32 \pm 0.5 \text{ MPa}$ ) (Fig. 4B,  $p < 0.05$ ). It can be due to the damage of the collagen structure in the scaffolds network. Because collagen is responsible for the skin's high Young's modulus so that at ages 15 to 30 years, the modulus is in the range of 0.32-4 MPa [72–74]. Obviously, the existence of non-bonded collagen, the lack of balance in stiffness and softness, or an excessive HA in scaffolds structure can be one of the reasons for the structural damage. Therefore, higher ultimate stress strength (UTS) and Young's modulus were recorded for S2 that indicates the scaffold containing 20 wt% of HA due to higher porosity offers higher resistance to the strain applied. (Fig. 4B and C). However, higher plastic limit and breaking strain% were for S1 due to the strength of the SF network structure (Fig. 4A and D).

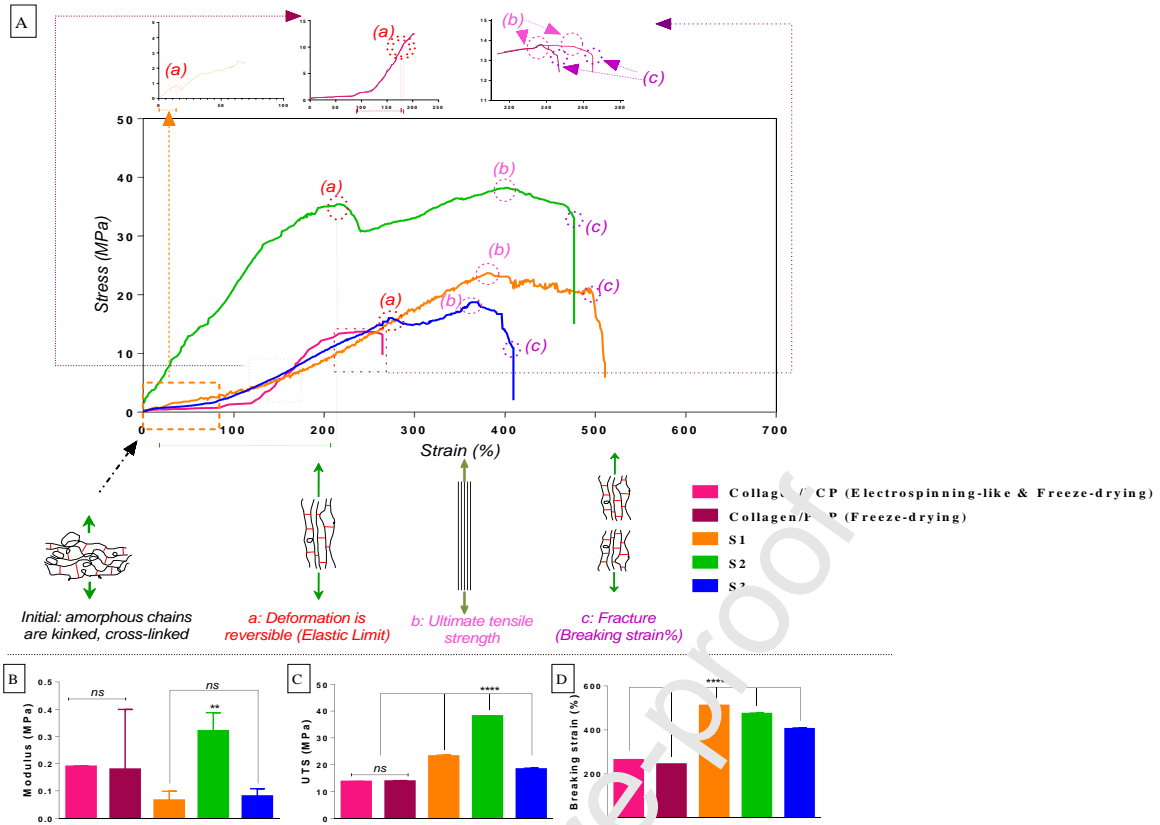


**Figure 4.** Mechanical behavior: A. The stress-strain curve of the scaffolds: (a) is elastic limit deformation that defined as a reversible deformation (similar to the word elasticity) and after removal of the applied stress (or load), the scaffold returns to its original size and shape (in this range the applied stress is directly proportional to the observed strain or elongation). The range of (ab) is plastic limit it means, if a scaffold is loaded beyond its elastic limit, it does not return to its original shape and size, i.e. a permanent deformation occurs (not reversible) hence (b) is ultimate stress strength. Hereafter, stress decreases because of the onset of the necking of scaffold that leads to the non-uniform plastic deformation before specimen fractures at point-c, so the range of (bc) is the fracture limit. B. Young's modulus (\*\*:  $p < 0.05$ ), C. Ultimate stress strength (UTS) (the parameter that describes the scaffold's strength) (\*\*\*\*:  $p < 0.001$ ), and D. Breaking strain% or elongation% (to indicate the scaffold's ductility under applied load before fracture) ( $p < 0.001$ ).

**Table 2.** The parameters of the tensile for 3D-scaffolds.

Parameters	S1	S2	S3	Collagen/PCP (Electrospinning- like and Freeze- drying)	Collagen/PCP (Freeze-drying)
Elastic limit %	$14.7 \pm 0.6$	$221.3 \pm 0.5$	$274.0 \pm 1.0$	$185.3 \pm 2.5$	$183.3 \pm 1.5$
UTS (MPa)	$23.2 \pm 0.4^a$	$38.1 \pm 0.1^a$	$18.4 \pm 0.3^a$	$13.7 \pm 0.02^b$	$13.8 \pm 0.2^{*,b}$
Breaking strain %	$510.6 \pm 0.5^a$	$473.6 \pm 3.2^a$	$404.6 \pm 4.5^a$	$263.6 \pm 1.5^a$	$244.3 \pm 0.06^{*,a}$

\* UTS (MPa) and breaking strain% for collagen/PCP (freeze-drying) scaffold were obtained from our previous study [5].

<sup>a</sup>The mean difference is significant at the 0.001 level.

<sup>b</sup>There is no significant difference between scaffolds ( $p > 0.001$ ).

### 3.5. Morphology and porosity% of scaffold

The morphological similarity of the engineered scaffold to native ECM is one of the main characteristics to design scaffolds. The existence of numerous pores ( $\mu\text{m}$ ) and consequently higher porosity% increases the scaffold ability as a supportive matrix for stem cell attachment [76]. Moreover, for various tissues (soft and hard), optimal pore diameter distributions in scaffolds differ according to tissue and materials used [58,77,78]. In this field, there is a wide range for pores diameter distributions in the scaffolds used for skin tissue to differentiate stem cells into fibroblasts and keratinocyte (15 to 160  $\mu\text{m}$ ) [79–83]. Hence, the selection of polymeric materials along with the design/fabrication techniques of scaffolds can play an important role in creating optimal pore and morphology similar to ECM of the skin [83–85]. Here, the hybrid porous scaffolds, which fabricated using injecting (electrospinning-like) along with the freeze-drying technique and freeze-drying method, confirm the mentioned items. So that, comparison of means pores diameter, pores diameter distributions and porosity% showed that the use of both methods of the electrospinning-like and the freeze-drying was led to a 16% reduction in the mentioned parameters, and a 1.5% increase of the porosity%, compared to the freeze-drying method ( $p < 0.05$ , Table 3). This can be explained by the injection of collagen into the PCP solution by the electrospinning-like method, which leads to gradually penetration of the water molecules into polymer solution and better interactions of collagen with hydrophobic polymer (PCL), and consequently stronger hydrogen bonding formation, creation of a denser structure with smaller pores size, and the more uniform distribution of pores diameter, via the freeze-drying method (with two-stages freezing process)(Fig. 5 and 6: A, B). The minor differences (non-significant) were also observed between S1 and collagen/PCP prepared by the electrospinning-like and freeze-drying methods, which can be due to the dominance of hydrophobic domains of SF and its  $\beta$ -sheet structure (Fig. 5A and C, Table 2,  $P > 0.001$ ).

Furthermore, the evaluation of SEM images illustrated a continuous interconnected 3D-network with the porous structure for S2 and S3 scaffolds, that their internal morphology was dependent on the ratio of the polysaccharide added (Fig. 5D and E). Indeed, the formation of numerous subordinate pores in the wall of the main pores after adding the HA leads to the improvement of inner network connectivity of pore, higher porosity% and more uniform morphology along with the lower-domain distribution of diameter, compared with other scaffolds (Fig. 6A-E, Table 3,  $P < 0.001$ ).

Our results showed also that the pores size of designed scaffolds was found to be within the range required for seeding stem cells and differentiate into skin cells such as keratinocyte which is related to the combination of natural and synthetic polymers [58,67,85,86].

However, relative to previous studies, the designed scaffolds in this research have the distribution of a more uniform diameter, which can be due to the combination of electrospinning-like and freeze-drying methods.

**Table 3.** The comparison of the scaffolds properties: pore diameter and porosity %.

Parameters			
Mean pore diameter ( $\mu\text{m}$ )	Pore diameter range ( $\mu\text{m}$ )	Mean porosity % $\pm$ SD	Ref.



Sample code	Collagen/PCP (Electrospinning-like and Freeze-drying)	~45 <sup>a, b, c</sup>	~ 18-101 <sup>b</sup>	93.0 ± 0.03 <sup>a, b</sup>	-
	Collagen/PCP (Freeze-drying)	~ 54 <sup>a, c</sup>	~ 13-118	91.6 ± 0.18 <sup>a</sup>	[5]
	S1 (SF/HA= 100:0)	~ 41 <sup>b, c</sup>	~ 14-90 <sup>b</sup>	93.3 ± 0.64 <sup>b</sup>	-
	S2 (SF/HA= 80:20)	~ 27 <sup>c</sup>	~ 8-52	97.5 ± 0.11	-
	S3 (SF/HA= 50:50)	~ 15 <sup>c</sup>	~ 6-33	99.0 ± 0.04	-

<sup>a</sup> The mean difference is significant at the 0.05 level.

<sup>b</sup> There is no significant difference between scaffolds ( $p > 0.001$ ).

<sup>c</sup> The mean difference is significant at the 0.001 level.

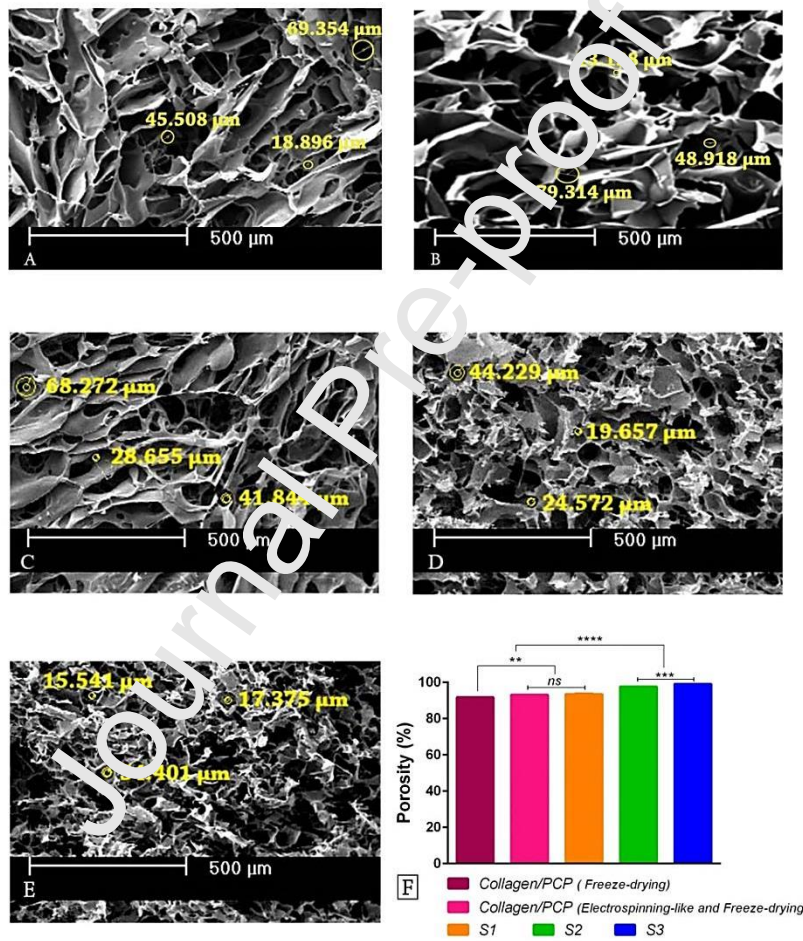


**Figure 5.** A-E: SEM images of scaffolds (before the seeding cells). F: The porosity% of scaffolds (\*\*:  $p < 0.05$ , \*\*\*:  $p < 0.01$ , \*\*\*\*:  $p < 0.001$ , and ns is defined as a non-significant difference). A to E images are related to collagen/PCP (Electrospinning-like and Freeze-drying), collagen/PCP (Freeze-drying), S1, S2, and S3 scaffolds, respectively.



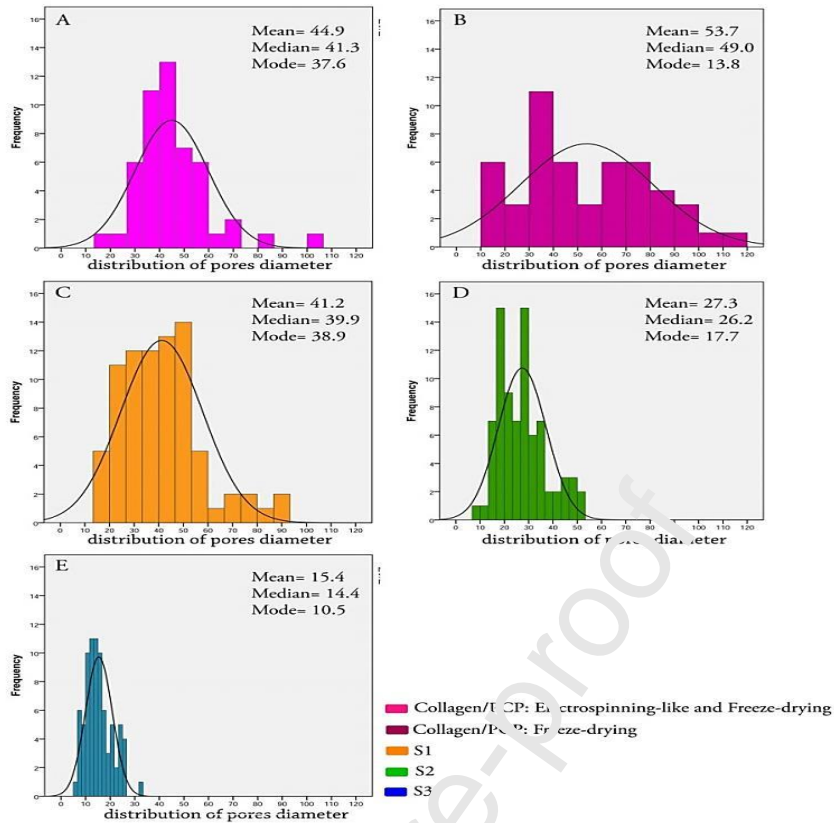


**Figure 6.** Histograms of diameter distribution for designed scaffolds.

### 3.6. Cellular adhesion and proliferation

After 5 h and 2 days of cell culture on the scaffold, the SEM images of scaffolds along with h-ASCs were observed to evaluate cell adhesion, distribution, and proliferation (Fig. 7A-H). The results revealed that the combination technique of the electrospinning-like and freeze-drying increases cellular adhesion and decreases the cell colony formation on the scaffolds (after 5 h) results in better interaction of cell-scaffolds and cell-cell, relative to the freeze-drying method (Fig. 7) (a) and (b). Actually, the lack of cell colony formation on the 3D-scaffold is considered as an important factor that can lead to less adhered cell loss on the surface and the promotion of cell differentiation, when scaffold structure is destroyed in cases such as enzymatic degradation and simple hydrolysis.

Adding SF and HA biomolecules into the collagen/PCP structure was also led to the improvement in the cellular adhesion, distribution, and proliferation (Fig. 7c-j). Moreover, the increase of HA content was promoted cell adhesion, so that more adhesion (after 5 h) was observed for S3 (Fig. 7c-e). This could be due to higher porosity% and more uniform morphology of the mentioned scaffold which led to better interactions of cell-to-scaffold [43,76], but this result does not necessarily increase cell proliferation. Indeed, pores facilitate and accelerate the loading of cells into scaffolds and porosity provides the internal sites for attachment [82]. However, an excessive decrease in the pores diameter or increase in the porosity can have a negative effect on the proliferation and differentiation of cells. Hence, the main problem is the creation of efficient interactions between the scaffolds and cells after primary adhesion, so that the small diameters of pores in scaffold meshes prohibit cell

penetration into the pores, so 3D-scaffold acts like a 2-dimensional (2D) support structure [87]. Under these circumstances, the high ability of cells to grow leads to fast proliferation and dispersion of cells in the 2D-scaffold and increases of pro-death signals due to the reduction of contact inhibition [88]. In this research, the application of PCL polymer has partially solved the problem of cell penetration, but the excessive increase in the weight ratio of HA (>20wt%) led to the smaller pores diameter, a decrease in-depth penetration of cells into the scaffold, and subsequent reduction of proliferation and differentiation, after 2 days (Fig. 7g-i). It is notable that S2 with 20 wt% of HA and porosity less than S3 (50 wt% of HA) showed more uniform distribution and better proliferation of h-ASCs onto the scaffold.

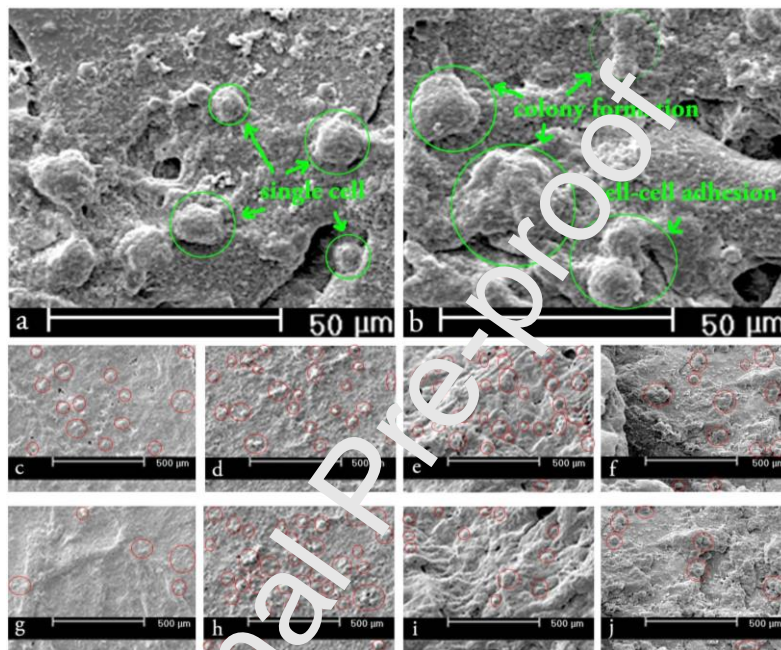


**Figure 7.** (a) and (b) are SEM images of collagen/PCP scaffolds along with h-ASCs for the combination technique of the electrospinning-like and freeze-drying, as well as the freeze-drying method, respectively. (c), (d), (e), and (f) are SEM images for S1, S2, S3, and collagen/PCP prepared with combination technique, respectively, after 5 h. Likewise, (g), (h), (i), and (j) are SEM images after 2 days.

### 3.9. Cell viability assay

The viability of cultured h-ASCs on designed scaffolds was assessed by MTT assay, after 1 and 2 days (Fig. 8A). No significant differences were observed between control and experimental groups ( $p > 0.01$ ), except S3 scaffold (after 24 h), that can be due to the higher degradation rate and excessive reduction of pores diameter in S3 scaffold which leads to reduced oxygen and nutrients transport to cells and decreased the number of viable cells. ( $p < 0.01$ ). Nevertheless, cell viability results for all scaffolds demonstrated more than 80% live cells. More cell viability% was also related to S2 at both day 1 and 2, compared to other scaffolds studied. This can be because of control of HA weight ratio, lower degradation%, suitable biomechanical properties, the balance of hydrophilic and hydrophobic groups, and consequently balance of stiffness and softness in the mentioned scaffold structure.

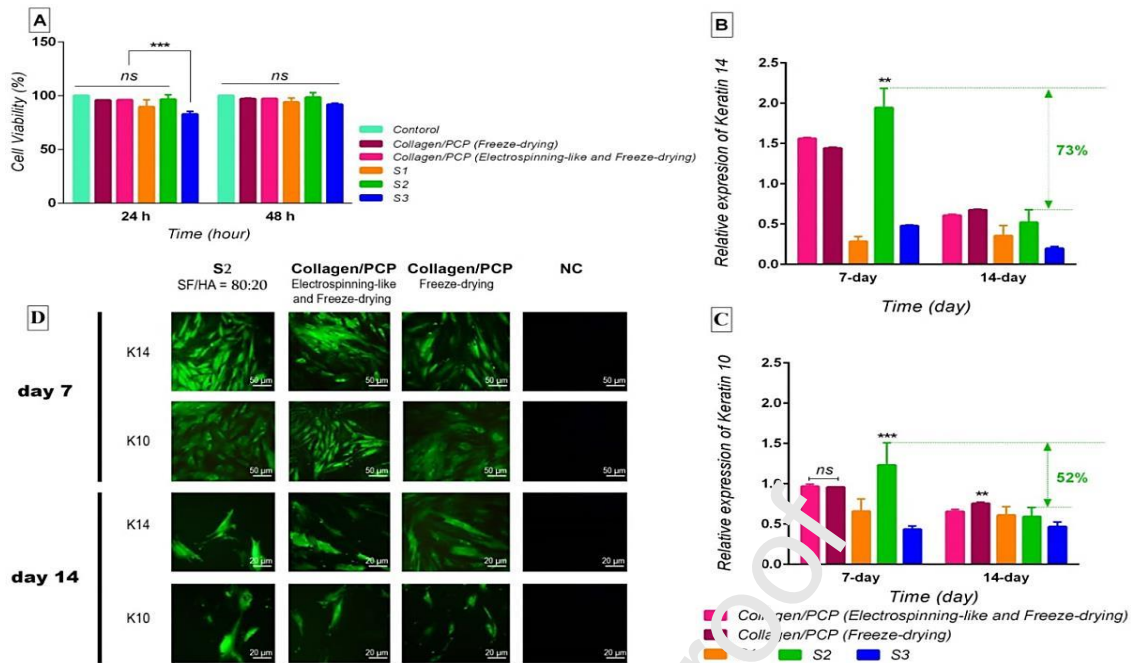


**Figure 8.** A: The viability of ASCs cultured on all five scaffolds, during 24 and 48 h. B and C: Expression of keratinocytes on all five scaffolds, after 7 and 14 days (B: KRT14 and C: KRT10). D: Immunocytochemical analysis of keratinocytes 14 and 10, on three scaffolds and negative control, after 7 and 14 days. \*\*\*:  $p < 0.01$ , \*\*:  $p < 0.05$ , ns: non-significant difference, and NC: negative control.

### 3.10. Real-time RT-PCR and immunocytochemistry analysis

The expression of early or late and induction of keratins by the basal cells are effective in the speed up wound healing. Thus, the ability of the skin tissue-engineered scaffolds which is dependent on the used materials and the specific design of the scaffold play an important role in keratinocytes differentiation from ASCs and timely keratins expression, because of keratins are expressed in specific patterns which are related to the type of tissue epithelial and stage of differentiation [89]. Hence, in this study expression of keratins 14 and 10 (as the most important keratins in basal and spinous (suprabasal) layers of the epidermis, as well as embryonic epithelial cells like hair follicle in the dermis, respectively [90–93]) on the designed scaffolds were investigated by RT-PCR and ICC-analysis. The results obtained after days 7 and 14 are summarized in Figures 8B-D.

It is notable that, the keratinocytes of 14 and 10 are an early differentiation marker, so the more expression must observe on day 7. Nonetheless, the expression level of KRT10 on day 7 is less than KRT14 and gradually induced in the following days (compared with KRT14 in day 14) [94]. This gradual process is related to the formation of the first suprabasal layer such as spinosum as a function of basal cells proliferation and induction of KRT10 during 14 days of wound healing (no scar) [95]. Therefore, S2 can probably be effective for this purpose due to the structure of the scaffold network and the regulation of the HA ratio. Figure 12 confirms the early expression of KRT10 and KRT14 on the mentioned scaffold.

As shown in Fig. 8B and C, except for the S1 scaffold, the differentiation of keratinocytes from h-ASCs was led to the early expression of KRT14 on all scaffolds so that more expression was recorded on the 7<sup>th</sup> day. Although there was a significant difference between

scaffolds in the expression level of KRT14 ( $p < 0.05$ ), that may be due to the more porosity, reduction in-depth penetration of cells into the scaffold, and decrease of their differentiation or proliferation.

In addition, collagen/PCP (electrospinning-like and freeze-drying) was led to ~8% increase in the KRT14 expression, compared with collagen/PCP (freeze-drying) on the 7<sup>th</sup> day. It could be due to the scaffold network and better interaction of cell-cell and cell-scaffold.

The results also showed h-ASCs culture on S3 was led to the lower expression level along with the late expression of KRT10 which can be due to the weaker physicochemical properties of scaffold and the type of cell-scaffold interactions.

Therefore, only three scaffolds of collagen/PCP(s) and S2 could mimic the differentiation and growth pattern of skin cells. However, after 7 days of culture on these three scaffolds, the more induction of keratinocytes 14 and 10 was observed on the S2 scaffold that could be due to the ratio of SF/HA and the regulation of HA content (as an induction factor of keratinocytes). After 14 days, the S2 scaffold showed a further decrease in the expression level of both keratinocytes (~73% and 52% respectively), compared with other scaffolds (Fig. 8B and C). This process plays an important role in the beginning of the early differentiation, upward stratification in skin layers for the formation of the suprabasal layer, and skin regeneration [96].

The ICC images confirmed the mentioned results (Fig 8D). It is notable that; based on the results of RT-PCR, the immunocytochemical study was carried out for only three scaffolds of collagen/PCP(s) and S2, due to the better results in keratinocytes induction and imitation of their differentiation pattern (early expression). The distinguishable phenotypical feature of keratinocytes was confirmed by ICC analysis (polygonal morphologies).

Notably, the significant differences observed in expression levels for KRT10 and KRT14 between the mentioned scaffolds and TCP (as the control group in the epidermal-induction medium), according to the  $2^{-\Delta\Delta C_t}$  method. Based on this method, expression levels of TCP will be equal to one and the rest of the groups will be compared relative to TCP.

Herein, after 7 days, the KRT14 expression on the S2 and collagen/PCP(s) was respectively recorded ~2 fold and ~1.5-fold the higher than TCP. It can be related to the limitations of 2D culture so that cells are distorted and flatten and cell-to-cell interactions are therefore virtually eliminated due to forming a surface of mono-layer. While a 3D-microenvironment with a porous network provides a tissue-like 3D structure and leads to cell permeation freely into the scaffold and improvement of cells behavior (adhesion, proliferation, and differentiation) [88,97,98]. Likewise, the KRT10 expression level on the S2 scaffold was ~1.5-fold greater than that on the TCP, while the expression of the mentioned keratinocyte was approximately equal between the control and collagen/PCP(s). It can be explained by the presence of SF/HA bio-complex with a volume ratio of 80:20 which acts as a key factor for keratinocytes induction.

This study suggests that the design of the hybrid scaffold as the engineered extracellular matrix not only can add to scaffold capabilities for cell adhesion, migration, proliferation, and differentiation into the tissue but also can be effective for early/late expression of predominant cells. Moreover, the combination of two techniques of electrospinning-like and freeze-drying can improve the mechanical and physical properties of the scaffold. The designed scaffolds in this research due to unique structure and characteristics indicated that



can potentially be effective for h-ASCs differentiation into keratinocytes in the absence of growth factor and promote biological signals.

These scaffolds because of having the proteoglycan (SF), linear polysaccharides (HA and chitosan), and collagen fibers provide a close resemblance to the native extracellular matrix [99–102] and can be as a regulator of cell function and a suitable substitute for wound healing. Accordingly, it seems that designed scaffolds in this study can be a good alternative for the amniotic membrane used in recent years for skin regeneration [103–106] however, further researches are needed, in this field.

Hence, the study of similarity of this scaffold with the biological substrates, such as amniotic membrane and its reform are the future studies that will reduce the inherent risks of biological materials.

#### 4. Conclusion

In the present study, a novel hybrid porous scaffold was designed that imitates not only the human skin functions but also can potentially induce epidermal keratinocytes to accelerate the wound healing process. This scaffold includes silk/hyaluronan copolymer modified by polyethylene glycol/chitosan/poly ( $\epsilon$ -caprolactone) biocomposite containing collagen. To create a coherent 3D network, the combination of the electrospinning-like and freeze-drying techniques was used as a new method for the preparation of scaffold. These scaffold properties were compared to the scaffold designed by the freeze-drying technique. The results demonstrated that the combination technique was led to a decrease in degradation% and mean pore diameter, an increase in porosity and breaking strain%, more regular swelling rate stable swelling behavior, the more uniform distribution of pores diameter and consequently more uniform distribution and better proliferation and differentiation of h-ASCs onto the scaffold. The evaluation of the different weight ratios (wt%) of SF/HA bio-complex (S1:100/0, S2:80/20, S3:50/50) showed that the increase of HA content (>20 wt%) was led to an increase in porosity% (99%) and pore diameter range. However, the scaffold consisting of the HA content of 20% (i.e. S2 scaffold) was indicated a stable swelling behavior, lower degradation% along with modulus of 0.32 MPa that defined for young skins. The comparison of data also revealed that the regulation of HA and SF content (in S2 scaffold) resulted in improved interactions of cell-to-cell and cell-to-scaffold (adhesion, cellular responses, proliferation, and differentiation) via promoting mechanotransduction signals and in the absence of growth factors. Such a scaffold as a promising substrate can be effective in managing the absorption of wound exudates and skin regeneration. However, complementary studies are required to test the efficacy of these scaffolds for wound healing in animal models.

#### Acknowledgements

We would like to express our deep appreciation to Dr. Arash Sarveazad for all his help and guidance that has given us over the past three years.

#### Declaration of Competing Interest

The authors declare that there are no conflicts of interest.

### Formatting of funding sources

This research did not receive any specific grant from funding agencies in the public, commercial, or not-for-profit sectors.

### Reference

- [1] M.D. Leonida, I. Kumar, *Bionanomaterials for Skin Regeneration*, Springer International Publishing, Cham, 2016.
- [2] C.L. Simpson, D.M. Patel, K.J. Green, *Nat. Rev. Mol. Cell Biol.* 12 (2011) 565–580.
- [3] M.G. Neuman, R.M. Nanau, L. Oruña, G. Coto, *J. Pharm. Pharm. Sci.* 14 (2011) 425–37.
- [4] A. Izadyari Aghmiuni, S. Heidari Keshel, F. Sefat, A. Akbarzadeh Kheyavi, *Int. J. Biol. Macromol.* 142 (2020) 668–679.
- [5] A. Izadyari Aghmiuni, M. Sharifzadeh Baei, S. Heidari Keshel, A. Akbarzadeh Kheyavi, *Fibers Polym.* 21 (2020) 33–44.
- [6] S.P. Tarassoli, Z.M. Jessop, A. Al-Sabah, N. Gao, S. Whitaker, S. Doak, I.S. Whitaker, *J. Plast. Reconstr. Aesthetic Surg.* 71 (2018) 615–623.
- [7] M.E. Furth, A. Atala, M.E. Van Dyke, *Biomaterials* 28 (2007) 5068–5073.
- [8] S. Balaji, S.G. Keswani, T.M. Crombleholme, *Adv. Wound Care* 1 (2012) 159–165.
- [9] E. Fuchs, V. Horsley, *Genes Dev.* 22 (2008) 976–985.
- [10] P. Zarrintaj, S. Manouchehri, Z. Ahmadi, M.K. Saeb, A.M. Urbanska, D.L. Kaplan, M. Mozafari, *Carbohydr. Polym.* 187 (2018) 66–84.
- [11] S.C. Johnson, Z.L. Smith, B.S. Sack, G.D. Steinberg, *Urol. Clin. North Am.* 45 (2018) 133–141.
- [12] B.S. Kim, Y.W. Kwon, J.-S. Kang, T. Park, G. Gao, W. Han, M.-B. Kim, H. Lee, J.H. Kim, D.-W. Cho, *Biomaterials* 168 (2018) 38–53.
- [13] K. Gwon, E. Kim, G. Tae, *Acta Biomater.* 49 (2017) 284–295.
- [14] Y.G. Illouz, *A. Sterodimas: Adipose Stem Cells and Regenerative Medicine*, Springer Berlin Heidelberg, 2011.
- [15] S.P. Huang, C.C. Hsu, C.C. Chang, C.H. Wang, S.C. Deng, N.T. Dai, T.M. Chen, J.Y.H. Chan, S.G. Chen, S.M. Huang, *Ann. Plast. Surg.* 69 (2012) 656–662.
- [16] W.K. Ong, S. Sugii, *Int. J. Biochem. Cell Biol.* 45 (2013) 1083–1086.
- [17] L. Frese, P.E. Dijkman, S.P. Hoerstrup, *Transfus. Med. Hemotherapy* 43 (2016) 268–274.
- [18] A. Sterodimas, J. de Faria, B. Nicaretta, I. Pitanguy, *J. Plast. Reconstr. Aesthetic Surg.* 63 (2010) 1886–1892.
- [19] I. Bružauskaitė, D. Bironaitė, E. Bagdonas, E. Bernotienė, *Cytotechnology* 68 (2016) 355–369.
- [20] K. Vyas, H. Vasconez, *Healthcare* 2 (2014) 356–400.
- [21] B. Nyambat, C.-H. Chen, P.-C. Wong, C.-W. Chiang, M.K. Satapathy, E.-Y. Chuang, *J. Mater. Chem. B* 6 (2018) 979–990.
- [22] S.P. Tarassoli, Z.M. Jessop, A. Al-Sabah, N. Gao, S. Whitaker, S. Doak, I.S. Whitaker, *J. Plast. Reconstr. Aesthetic Surg.* 30 (2017) 6213–6220.
- [23] H. Lu, T. Hoshiba, N. Kawazoe, I. Koda, M. Song, G. Chen, *Biomaterials* 32 (2011) 9658–9666.
- [24] G.D. Mogoşanu, A.M. Grumezescu, *Int. J. Pharm.* 463 (2014) 127–136.
- [25] G. Huang, F. Li, X. Zhao, Y. Ma, Y. Li, M. Lin, G. Jin, T.J. Lu, G.M. Genin, F. Xu, *Chem. Rev.* 117 (2017) 12764–12850.
- [26] Y. Ma, M. Lin, G. Huang, Y. Li, S. Wang, G. Bai, T.J. Lu, F. Xu, *Adv. Mater.* 30 (2018) 1705911.
- [27] F. Ghorbani, A. Zamanian, H. Nojehdehian, *Mater. Sci. Eng. C* 77 (2017) 159–172.



- [28] S. Ahn, H. Yoon, G. Kim, Y. Kim, S. Lee, W. Chun, *Tissue Eng. Part C Methods* 16 (2010) 813–820.
- [29] M.G. Haugh, C.M. Murphy, R.C. McKiernan, C. Altenbuchner, F.J. O'Brien, *Tissue Eng. Part A* 17 (2011) 1201–1208.
- [30] T. Du, Z. Chen, H. Li, X. Tang, Z. Li, J. Guan, C. Liu, Z. Du, J. Wu, *Int. J. Biol. Macromol.* 82 (2016) 580–588.
- [31] L. He, C. Mu, J. Shi, Q. Zhang, B. Shi, W. Lin, *Int. J. Biol. Macromol.* 48 (2011) 354–359.
- [32] R. Huang, W. Li, X. Lv, Z. Lei, Y. Bian, H. Deng, H. Wang, J. Li, X. Li, *Biomaterials* 53 (2015) 58–75.
- [33] X. Liu, N. Dan, W. Dan, J. Gong, *Int. J. Biol. Macromol.* 82 (2016) 989–997.
- [34] F.G. Omenetto, D.L. Kaplan, *Science* 329 (2010) 528–31.
- [35] B. Kundu, R. Rajkhowa, S.C. Kundu, X. Wang, *Adv. Drug Deliv. Rev.* 65 (2013) 457–470.
- [36] T.W. Chung, Y.L. Chang, *J. Mater. Sci. Mater. Med.* 21 (2010) 1343–1351.
- [37] N.A. Ayoub, J.E. Garb, R.M. Tinghitella, M.A. Collin, C.Y. Hayashi, *PLoS One* 2 (2007) e514.
- [38] Y. Zhang, H. Yang, H. Shao, X. Hu, *J. Biomed. Biotechnol.* 2010 (2010) 1–8.
- [39] E. Bini, D.P. Knight, D.L. Kaplan, *J. Mol. Biol.* 335 (2004) 27–40.
- [40] G. Kogan, L. Soltés, R. Stern, P. Gemeiner, *Biotechnol. J.* 20 (2006) 17–25.
- [41] N. Volpi, J. Schiller, R. Stern, L. Soltés, *Curr. Med. Chem.* 16 (2009) 1718–1745.
- [42] A.C. Petrey, C.A. de la Motte, *Front. Immunol.* 5 (2014) 1–14.
- [43] J. Lam, N.F. Truong, T. Segura, *Acta Biomater.* 10 (2014) 1571–1580.
- [44] K.T. Dicker, L.A. Gurski, S. Pradhan-Bhatt, R.L. Witt, M.C. Farach-Carson, X. Jia, *Acta Biomater.* 10 (2014) 1558–1570.
- [45] D.L. Hern, J.A. Hubbell, *J. Biomed. Mater. Res.* 39 (1998) 266–276.
- [46] K.L. Moffat, K. Goon, F.T. Moutos, B.T. Fister, S.J. Oswald, X. Zhao, F. Guilak, *Macromol. Biosci.* 18 (2018) 1800140.
- [47] *J. Biomed. Mater. Res. Part A* 106 (2018) 2382–2393.
- [48] Y. Ma, Y. Ji, G. Huang, K. Ling, X. Zhang, F. Xu, *Biofabrication* 7 (2015) 44105.
- [49] Y. Ma, Y. Ji, T. Zhong, W. Wan, Q. Yang, A. Li, X. Zhang, M. Lin, *ACS Biomater. Sci. Eng.* 3 (2017) 3534–3545.
- [50] S. Eshraghi, S. Das, *Acta Biomater.* 6 (2010) 2467–2476.
- [51] M.A. Woodruff, D.W. Huttmacher, *Prog. Polym. Sci.* 35 (2010) 1217–1256.
- [52] K.T. Shalumon, K.H. Anulekha, K.P. Chennazhi, H. Tamura, S. V. Nair, R. Jayakumar, *Int. J. Biol. Macromol.* 48 (2011) 571–576.
- [53] E.J. Chong, T.T. Phan, I.J. Kim, Y.Z. Zhang, B.H. Bay, S. Ramakrishna, C.T. Lim, *Acta Biomater.* 3 (2007) 321–329.
- [54] G.H. Kim, *J. Polym. Sci. Part B Polym. Phys.* 44 (2006) 1426–1433.
- [55] Q.L. Loh, C. Chong, *Tissue Eng. Part B Rev.* 19 (2013) 485–502.
- [56] W.W. Thein-Han, R.D.K. Misra, *Acta Biomater.* 5 (2009) 1182–1197.
- [57] J. Venkatesan, I. Bhatnagar, S.K. Kim, *Mar. Drugs* 12 (2014) 300–316.
- [58] D. Atila, D. Keskin, A. Tezcaner, *Carbohydr. Polym.* 133 (2015) 251–261.
- [59] U.J. Kim, J. Park, H. Joo Kim, M. Wada, D.L. Kaplan, *Biomaterials* 26 (2005) 2775–2785.
- [60] K.K. Nayak, P. Gupta, *Int. J. Biol. Macromol.* 81 (2015) 1–10.
- [61] I. Adekogbe, A. Ghanem, *Biomaterials* 26 (2005) 7241–7250.
- [62] X. Zhao, X. Sun, L. Yildirimer, Q. Lang, Z.Y. (William) Lin, R. Zheng, Y. Zhang, W. Cui, N. Annabi, A. Khademhosseini, *Acta Biomater.* 49 (2017) 66–77.
- [63] (n.d.).
- [64] Q. Tan, S. Li, J. Ren, C. Chen, *Int. J. Mol. Sci.* 12 (2011) 890–904.
- [65] B.H. León-Mancilla, M.A. Araiza-Téllez, J.O. Flores-Flores, M.C. Piña-Barba, *J. Appl. Res. Technol.* 14 (2016) 77–85.
- [66] A. Vasconcelos, A.C. Gomes, A. Cavaco-Paulo, *Acta Biomater.* 8 (2012) 3049–3060.
- [67] J. Ramana Ramya, K. Thanigai Arul, P. Sathiamurthi, K. Asokan, S. Narayana Kalkura, *Ceram. Int.* 42 (2016) 11045–11054.
- [68] X. Hu, Q. Lu, L. Sun, P. Cebe, X. Wang, X. Zhang, D.L. Kaplan, *Biomacromolecules* 11 (2010) 3178–3188.

- [69] H. Zhang, L. Zhou, W. Zhang, *Tissue Eng. Part B Rev.* 20 (2014) 492–502.
- [70] Z. She, C. Jin, Z. Huang, B. Zhang, Q. Feng, Y. Xu, *J. Mater. Sci. Mater. Med.* 19 (2008) 3545–3553.
- [71] Y. Zheng, A.F.T. Mak, *IEEE Trans. Rehabil. Eng.* 7 (1999) 257–267.
- [72] A.J. Gallagher, A. Ní Annaidh, K. Bruyère, E. Al., in: *IRCOBI Conf.*, 2012, pp. 494–502.
- [73] A. Ní Annaidh, K. Bruyère, M. Destrade, M.D. Gilchrist, M. Otténio, *J. Mech. Behav. Biomed. Mater.* 5 (2012) 139–148.
- [74] K. A, L. A, *J. Mater. Sci. Eng.* 5 (2016).
- [75] A. Karimi, M. Haghghatnama, A. Shojaei, M. Navidbakhsh, A. Motevalli Haghi, S.J. Adnani Sadati, *Proc. Inst. Mech. Eng. Part L J. Mater. Des. Appl.* 230 (2016) 418–425.
- [76] F.H. Zulkifli, F.S.J. Hussain, M.S.B.A. Rasad, M. Mohd Yusoff, *Carbohydr. Polym.* 114 (2014) 238–245.
- [77] C.M. Murphy, M.G. Haugh, F.J. O’Brien, *Biomaterials* 31 (2010) 461–466.
- [78] M. Kim, G. Kim, *RSC Adv.* 5 (2015) 26954–26964.
- [79] J. Ma, H. Wang, B. He, J. Chen, *Biomaterials* 22 (2001) 331–336.
- [80] W.F. Lee, Y.J. Chen, *J. Appl. Polym. Sci.* 82 (2001) 2487–2496.
- [81] J. Yang, G. Shi, J. Bei, S. Wang, Y. Cao, Q. Shang, G. Yan, W. Wang, *J. Biomed. Mater. Res.* 62 (2002) 438–446.
- [82] D.E. López Angulo, P.J. do Amaral Sobral, *Int. J. Biol. Macromol.* 92 (2016) 645–653.
- [83] T.W. Wang, H.C. Wu, Y.C. Huang, J.S. Sun, F.H. Lin, *Ann. Organs* 30 (2006) 141–149.
- [84] F.J. O’Brien, B.A. Harley, I.V. Yannas, L.J. Gibson, *Biomaterials* 26 (2005) 433–441.
- [85] X. Zhu, W. Cui, X. Li, Y. Jin, *Biomacromolecules* 9 (2008) 1795–1801.
- [86] L. Ma, C. Gao, Z. Mao, J. Zhou, J. Shen, X. Hu, C. Han, *Biomaterials* 24 (2003) 4833–4841.
- [87] A.K. Ekaputra, G.D. Prestwich, S.M. Cool, T.W. Huttmacher, *Biomacromolecules* 9 (2008) 2097–2103.
- [88] A. Szentivanyi, T. Chakradeo, H. Zernoch, B. Glasmacher, *Adv. Drug Deliv. Rev.* 63 (2011) 209–220.
- [89] R. Moll, M. Divo, L. Langbein, *Histochem. Cell Biol.* 129 (2008) 705–733.
- [90] L. Cassimeris, G. Plopper, V.R. Lingappa, *Lewin’s CELLS*, Jones & Bartlett Learning, LLC, 2011.
- [91] G. Guasch, *Biol. Eng. Stem Cell. Niches* (2017) 127–143.
- [92] A.M.B. Tadeu, V. Horsley, in: *Curr. Top. Dev. Biol.*, 1st ed., Elsevier Inc., 2014, pp. 109–131.
- [93] T. Drewa, R. Joachimiak, A. Bajek, M. Gagat, A. Grzanka, M. Bodnar, A. Marszalek, R. Debski, P. Chłosta, *Int. J. Urol.* 20 (2013) 537–542.
- [94] E.B. Lane, W.H.I. McLean, *J. Pathol.* 204 (2004) 355–366.
- [95] M. Santos, J.S.M. Faranjo, A. Bravo, A. Ramirez, J.L. Jorcano, *J. Biol. Chem.* 277 (2002) 19122–19130.
- [96] L. Zhang, in: *Keratin*, IntechOpen, 2018, p. 13.
- [97] S. Ortinau, J. Schmich, S. Block, A. Liedmann, L. Jonas, D.G. Weiss, C.A. Helm, A. Rolfs, M.J. Frech, *Biomed. Eng. Online* 9 (2010) 70.
- [98] N. Davidenko, C.F. Schuster, D. V. Bax, R.W. Farndale, S. Hamaia, S.M. Best, R.E. Cameron, *J. Mater. Sci. Mater. Med.* 27 (2016) 148.
- [99] S. Türkkan, D. Atila, A. Akdağ, A. Tezcaner, *J. Biomed. Mater. Res. Part B Appl. Biomater.* 106 (2018) 2625–2635.
- [100] Y.R. Park, H.W. Ju, J.M. Lee, D.K. Kim, O.J. Lee, B.M. Moon, H.J. Park, J.Y. Jeong, Y.K. Yeon, C.H. Park, *Int. J. Biol. Macromol.* 93 (2016) 1567–1574.
- [101] N. Bhardwaj, W.T. Sow, D. Devi, K.W. Ng, B.B. Mandal, N.-J. Cho, *Integr. Biol.* 7 (2015) 142–142.
- [102] A.A. Mahmoud, A.H. Salama, *Eur. J. Pharm. Sci.* 83 (2016) 155–165.
- [103] B. Farhadhosseinabadi, M. Farahani, T. Tayebi, A. Jafari, F. Biniazan, K. Modaresifar, H. Moravvej, S. Bahrami, H. Redl, L. Tayebi, H. Niknejad, *Artif. Cells, Nanomedicine, Biotechnol.* 0 (2018) 1–10.
- [104] M. Serra, L. Roseti, A. Bassi, *Methods Mol. Biol.* 1283 (2015) 161–9.
- [105] E. Taghiabadi, B. Beiki, N. Aghdami, A. Bajouri, in: *Vlakna a Text.*, 2018, pp. 79–81.

- [106] S. V. Murphy, A. Skardal, L. Song, K. Sutton, R. Haug, D.L. Mack, J. Jackson, S. Soker, A. Atala, *Stem Cells Transl. Med.* 6 (2017) 2020–2032.

Journal Pre-proof

**Author statement**

All authors discussed the results and contributed to the final manuscript.

Journal Pre-proof

**Declaration of interests**

The authors declare that they have no known competing financial interests or personal relationships that could have appeared to influence the work reported in this paper.

The authors declare the following financial interests/personal relationships which may be considered as potential competing interests:

Journal Pre-proof

**Highlights**

- The design of an ECM-like scaffold is the main challenge in skin tissue engineering.
- Fabrication techniques of scaffold and its constituent polymers play an important role in mimicking the structural network and function of ECM.
- The combination techniques can provide a more coherent 3D-network for the scaffold.
- Such a scaffold can increase mechanical signals transduction into the biological signals and induct h-ASC differentiation into keratinocytes.